# Josephson coupling across a long single-crystalline Cu nanowire

O. V. Skryabina,[1,2] S. V. Egorov,[1,3] A. S. Goncharova,[4] A. A. Klimenko,[4] S. N. Kozlov,[1,5] V. V. Ryazanov,[1,2,3,6] S. V. Bakurskiy,[2,6,7] M. Yu. Kupriyanov,[2,6,7,8] A. A. Golubov,[2,9] K. S. Napolskii,[4,10] and V. S. Stolyarov[1,2,5,8,a)]
[1]*Institute of Solid State Physics RAS, 142432 Chernogolovka, Russia*
[2]*Moscow Institute of Physics and Technology, 141700 Dolgoprudny, Russia*
[3]*Russian Quantum Center, Skolkovo, Moscow Region, 143025, Russia*
[4]*Department of Materials Science, MSU, 119991 Moscow, Russia*
[5]*Fundamental Physical and Chemical Engineering Department, MSU, 119991 Moscow, Russia*
[6]*National University of Science and Technology MISIS, 4 Leninsky prosp., 119049 Moscow, Russia*
[7]*Skobeltsyn Institute of Nuclear Physics, MSU, 119991 Moscow, Russia*
[8]*Solid State Physics Department, KFU, 420008 Kazan, Russia*
[9]*Faculty of Science and Technology and MESA+ Institute of Nanotechnology, 7500 AE Enschede, The Netherlands*
[10]*Department of Chemistry, MSU, 119991 Moscow, Russia*

(Received 3 December 2016; accepted 17 May 2017; published online 1 June 2017)

We report on a fabrication method and electron-transport measurements for submicron Josephson junctions formed by Cu nanowires coupling to superconducting planar Nb electrodes. The Cu nanowires with a resistivity of $\rho_{Cu} \simeq 1\ \mu\Omega$ cm at low temperatures consisting of single-crystalline segments have been obtained by templated electrodeposition using anodic aluminum oxide as a porous matrix. The current-voltage characteristics of the devices have been studied as a function of temperature and magnetic field. For all junctions, the critical current monotonically decreases with a magnetic field. The measured temperature and magnetic field dependencies are consistent with the model for one-dimensional diffusive superconductor/normal metal/superconductor (SNS) Josephson junctions within the quasiclassical theory of superconductivity. *Published by AIP Publishing.*
[http://dx.doi.org/10.1063/1.4984605]

The Josephson variable thickness bridge (VTB), which consists of two superconducting (S) banks connected by a thin narrow normal-metal (N) film, is a subject of intensive experimental[1–18] and theoretical[19–22] studies. N-nanobridge fabrication by means of e-beam, thermal, or magnetron deposition in an ultra-high vacuum through lithography masks[1–17] as well as by means of electrodeposition inside a mesoporous template with 1D channels[23,24] or CVD technique[25] usually results in the formation of polycrystalline or amorphous N-nanobridges with a small electron mean free path and diffusion coefficient $D$. This leads to reduction of important parameters such as the superconducting coherence length in the N segment of an superconductor/normal metal/superconductor (SNS) junction, $\xi_N \sim D^{1/2}$.

Fabrication of single-crystalline N-nanowires with lengths above one micrometer by the electrochemical, hydrothermal, or CVD techniques was reported in Refs. 26–31. The use of such nanowires for VTB device fabrication requires implementation of *ex situ* technology. Previously, such a technology was used in Ref. 27 for the fabrication of Au-nanowire-based VTB structures with low interface resistance but a large nanowire resistivity of 14 $\mu\Omega$ cm. In this work, we develop the fabrication technology of VTB based on Nb electrodes and single-crystalline Cu nanowires. Nanowires have a low resistivity on the order of 1 $\mu\Omega$ cm and the Nb/Cu specific interface resistance is of the order of $10^{-11}\ \Omega\ \text{cm}^2$ that is at the level typical to the *in situ* fabricated structures.[32] The fabricated junctions exhibit relatively high critical temperature and Josephson critical current density. The experimental data are in good agreement with the model based on the quasiclassical theory of superconductivity.[33]

Copper nanowires were prepared by metal electrodeposition inside the anodic alumina template, as described elsewhere.[34–36] Cu electrodeposition was carried out using an electrolyte containing 1 M $CuSO_4$, 0.5 M $H_2SO_4$, and 0.01 M HCl at a deposition potential of 0.05 V versus Ag/AgCl. In order to extract Cu nanowires, the oxide matrix was selectively dissolved in an oxidant-free alkaline solution (see supplementary material for more details). The scanning electron microscopy (SEM) image demonstrates the formation of several micrometer long nanowires with a uniform diameter along their length (see Fig. 1). According to the statistical analysis of SEM images, the diameter of Cu nanowires in the obtained suspension varies from 100 to 170 nm due to the dispersion of pores in the AAO template. Variations in the diameter along the length of a single nanowire do not exceed 10 nm. The transmission electron microscopy (TEM) image and selected area electron diffraction (SAED) pattern reveal that copper nanowires have single crystal structures (see insets in Fig. 1).

The process of Nb/Cu-nanowire/Nb VTB fabrication started with seeding Cu nanowires from suspension on the surface of the marked $Si/SiO_2$(270 nm) substrate by spin-coating. Then, the substrate was covered with PMMA e-beam resist and the windows were made by means of electron lithography for subsequent Nb film deposition. Prior to the metal deposition, the samples were etched in the argon plasma to remove organic and contaminating residuals from

a)Electronic mail: vasiliy@travel.ru

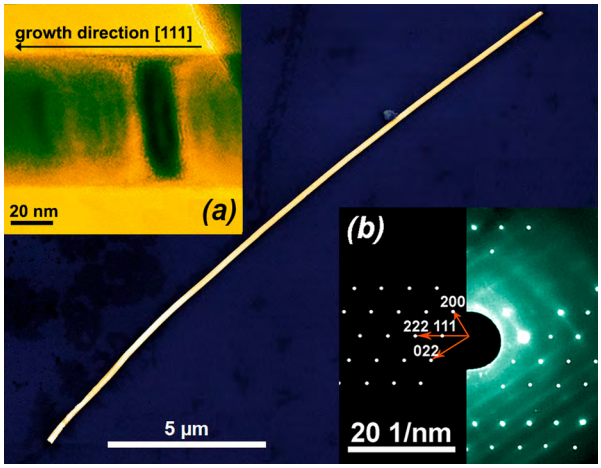


FIG. 1. SEM image of an individual copper nanowire; inset (a) is a TEM image and inset (b) is a SAED pattern for copper nanowires, prepared by the templated electrodeposition technique.

the nanowire surface. After that, a 240 nm thick Nb layer was deposited by magnetron sputtering in the same vacuum cycle. Initially, the chamber was pumped down to $5 \times 10^{-9}$ mbar, and then filled with pure argon (99.995) up to a pressure of $4 \times 10^{-3}$ mbar. Finally, Nb electrodes were formed by the lift-off process. The developed technique of SNS VTB fabrication allows one to get an acceptable value of Nb/Cu-nanowire interface resistance and to avoid oversputtering of the material along the weak link, which usually happens during the fabrication of electrical contacts by means of the focused ion beam (FIB) technique.[37]

Figures 2(a), 2(b), and 2(c) demonstrate the SEM images of Nb/Cu-nanowire/Nb junctions with different lengths of the weak link. The diameters of the Cu nanowires, $d$, and the spaces between Nb electrodes, $L$, of the junctions are given in Table I.

The transport properties of Nb/Cu-nanowire/Nb junctions were studied in two- and four-probe geometries [Fig. 2(d)]. The superconducting transition temperature $T_c$ of the Nb layer was 8.3 K [Fig. 2(e)]. The transport measurements were performed in a dilution refrigerator at temperatures down to 0.02 K using the 4-probe scheme. A He-4 cryostat equipped with a superconducting solenoid providing the magnetic field up to 1.4 T was used for the 2-probe transport measurement scheme at temperatures down to 1.2 K. The samples were mounted on a holder such that the magnetic field was perpendicular to the nanowire. All measurement lines were equipped with low temperature RC filters. The measurement results are presented in Figs. 3 and 4.

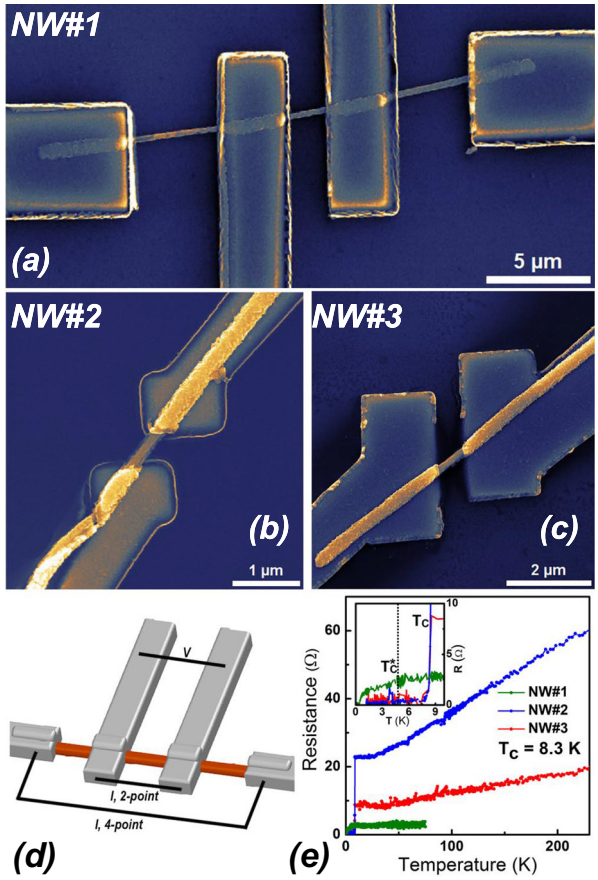


FIG. 2. (a), (b), (c) SEM images of three Josephson junctions Nb/Cu-nanowire/Nb with different lengths and nanowire diameters. (d) Sketch of the measurement geometry. (e) Superconducting transitions with $T_c = 8.3$ K. The inset shows the low-temperature region of resistance transitions, where a gradual decrease in resistance of the sample NW#1 below $T_c^* \approx 5$ K is visible (the green curve).

Figure 3(a) shows the current-voltage characteristics (IVC) of samples NW#1 (green line) at 0.02 K and NW#2 (blue line) and NW#3 (red line) at 1.2 K. The shape of the curves is typical for the SNS Josephson junctions with a large transparency of the SN interfaces. The contact resistances $R_B^{total}$ were obtained by comparing 2-probe and 4-probe measurements and were found to be 0.08 Ω and 0.12 Ω for NW#2 and NW#3, respectively. Here, $R_B^{total}$ is the sum of the contact resistances of the left and right SN interfaces. The IVCs demonstrate clearly pronounced critical currents $I_{c1} = 0.7$ μA, $I_{c2} = 30$ μA, and $I_{c3} = 17$ μA for NW#1, NW#2, and NW#3, respectively. At high voltages, the IVCs do not exhibit any signatures of excess or deficit currents. This is in agreement

TABLE I. The transport properties of samples were studied in two-probe (2-p) and four-probe (4-p) geometries at 1.2 K and 20 mK, respectively. Sample parameters: $L$ is a space between Nb-electrodes and $d$ is a nanowire diameter (they have been determined from SEM images). $I_c$ is the critical current, and $R$ is the normal state resistance of the weak links; $\rho$ is the Cu nanowire resistivity (the latter was measured experimentally for 4-p samples and was calculated as a result of fitting of magnetic and temperature dependencies for 2-p samples by Usadel equations). $D$ and $\xi_N$ are the calculated diffusion coefficient and coherence length, respectively. $T_c$ and $T_c^*$ are the critical temperature of Nb electrodes and effective critical temperature of the proximized part of the nanowire under the Nb electrode taken from fit; $\gamma_B = R_B/\rho\xi_N$, where $R_B$ is the SN interface specific resistance.

| Sample | Geometry | $L_{wl}$ (nm) | $d$ (nm) | $R$ (Ω) | $\rho$ (μΩ cm) | $D$ (m$^2$/s) | $\xi_N$ (nm) | $I_c$ (μA) | $T_c/T_c^*$ (K) | $\gamma_B$ |
|---|---|---|---|---|---|---|---|---|---|---|
| NW#1 | 4-p, 20 mK | 1765 ± 116 | 108 ± 10 | 2.20 | 1.14 ± 0.26 | 0.03 | 66 | 0.7 | … | … |
| NW#2 | 2-p, 1.2 K | 609 ± 112 | 114 ± 6 | 0.46 | 0.77 | 0.04 | 80 | 30 | 8.3/5.0 | 4.4 |
| NW#3 | 2-p, 1.2 K | 671 ± 105 | 168 ± 9 | 0.37 | 1.18 | 0.03 | 65 | 17 | 8.3/5.2 | 4.2 |

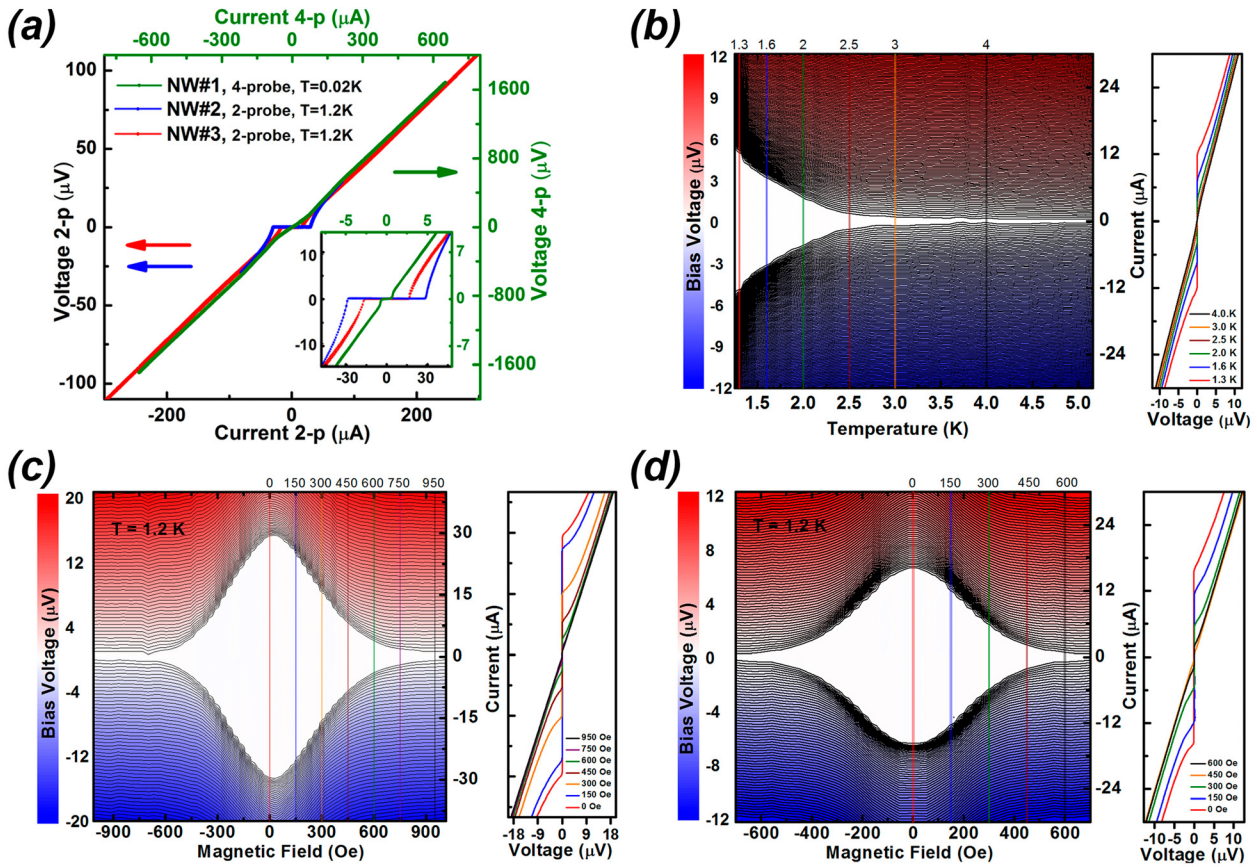


FIG. 3. Electric-transport characteristics for the Nb/Cu-nanowire/Nb junctions: (a) green, blue, and red lines are $I(V)$ characteristics of the samples NW#1, NW#2, and NW#3, respectively; the inset is a zoom of $I(V)$ plots. (b) Dependence of $I(V)$ curves on the temperature for the sample NW#3. (c) and (d) $I(V)$ dependencies as a function of perpendicular magnetic field $H$ for the NW#2 and NW#3, respectively; the measurement temperature is $T = 1.2$ K. $I(V)$ curves shown to the right of the panels (b), (c), (d) correspond to the sections of the 3D graphs at certain temperature or magnetic field values.

with theoretical predictions[19] for long SNS junctions. Note that in contrast to some previous studies of superconducting planar junctions (see Ref. 17 and references therein), the IVC of the sample NW#1 is not hysteretic at temperatures down to 20 mK. This fact might be caused by the possibility for the hot electrons to escape from the central part of the wire connecting the voltage probes in our sample.

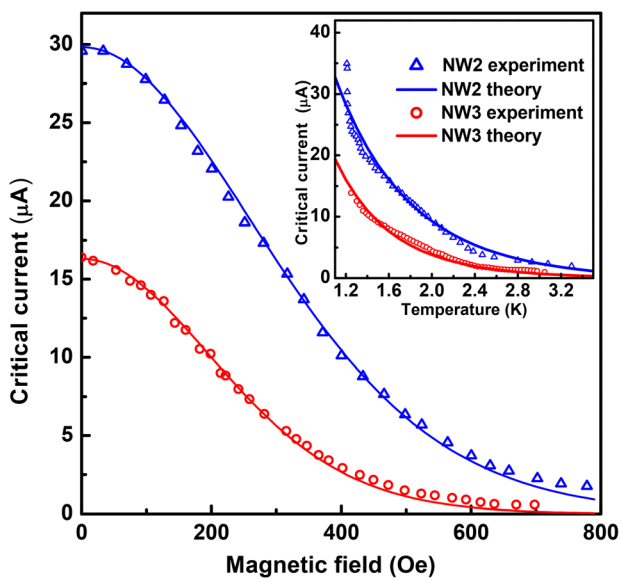


FIG. 4. Magnetic field dependencies of the critical current for the samples NW#2 (blue triangles) and NW#3 (red circles) at $T = 1.2$ K in comparison with theoretical fits (red and blue solid lines, respectively). The inset shows the temperature dependencies of the critical current with fits for the both samples at zero field.

The weak link normal resistance $R_1 = 2.2\ \Omega$ for sample NW#1 was obtained using the 4-probe scheme. It follows that the resistivity $\rho_{Cu} = 1.14 \pm 0.26\ \mu\Omega$ cm of the Cu weak link is comparable to the values of $\rho$ experimentally achieved earlier for Cu nanowire systems[28] at the liquid helium temperature.

Figure 3(b) presents the temperature dependence of the IVCs shape, while Figs. 3(c) and 3(d) show the evolution of IVCs of the samples NW#2 and NW#3 in external magnetic field $H$, applied perpendicular to the junction plane. Due to the high critical field of the Nb electrodes, a noticeable critical current of the samples is measured up to the magnetic field $H = 1000$ Oe. A monotonic decrease in the measured critical current $I_c$ with an increase in magnetic field is observed. Complete suppression of $I_c$ occurs at about 1 T. Earlier, similar magnetic field dependencies of the critical current were observed in planar Nb/Au/Nb and Al/Au/Al junctions along with InAs nanowire-based junctions.[7,38,39] The observed monotonous decrease in $I_c$ with increasing magnetic field can be explained by the magnetic pair breaking effect in Josephson junctions with large length/width ratio and the width of the normal nanowire comparable with the magnetic length $\xi_H = (\Phi_0/H)^{1/2}$ (where $H$ is the magnetic field and $\Phi_0$ the flux quantum), as predicted by Bergeret and Cuevas.[20,21]

In Fig. 4, the data for the samples NW#2 and NW#3 (open triangles and circles, respectively) are compared with the results of theoretical calculations in the frame of the Usadel equations.[33] As a model for the junctions investigated using 2-probe geometry, we consider an SINIS type structure where I is the interface barrier between the Nb electrode and the Cu nanowire described by the parameter $\gamma_B = R_B/\rho\xi_N$. Within this model, we have numerically calculated supercurrents using the parameters summarized in Table I. The effect of the magnetic field was taken into account by renormalization the quasiclassical energy according to the approach Refs. 20 and 21. The mean free path $l_e$, the diffusion coefficient $D = \frac{1}{3} v_F l_e$, and the coherence length $\xi_N = \sqrt{\hbar D/2\pi k_B T_c}$ for the Cu nanowires were estimated from the $\rho$-value fitting using literature data for the Fermi velocity $v_F$ in Cu and the carrier density $n_{Cu}$, providing $\xi_N = 80$ nm and $l_e = 84$ nm for the sample NW#2 and $\xi_N = 64$ nm and $l_e = 55$ nm for the sample NW#3. In both samples, $l_e$ is comparable to the wire diameter and exceeds the value of 19 nm reported for Au nanowires in Ref. 27.

A good quantitative fit of the data was obtained using $\gamma_B$ as a fitting parameter. The obtained value $\gamma_B = 4$ (see Table I) corresponds to the relatively low Nb/Cu specific interface resistance on the order of $10^{-11}$ $\Omega$ cm$^2$ at the level typical to the *in situ* fabricated structures.[32] At the same time, due to the finite value of $\gamma_B$, the superconducting gap induced in the Cu nanowire is smaller than the bulk gap of Nb. Therefore, the theoretical curves shown in Fig. 4 were calculated using a reduced transition temperature of the combined Cu/Nb electrode $T_c^* = 5$ K, in agreement with the behavior of the resistance of the sample NW#1 shown in the inset to Fig. 2(e).

In summary, we have developed a method of fabrication for the Nb/Cu-nanowire/Nb Josephson junctions and characterized these nanostructures. By taking advantage of Nb as a superconducting electrode and a single-crystalline Cu nanowire as a barrier, we demonstrate a measurable Josephson supercurrent up to a relatively high temperature of 3.5 K. The resistivity of the copper nanowires $\rho_{Cu} \sim 1$ $\mu\Omega$ cm is lower when compared to the values previously achieved in nanowire-based VTB structures. The measurements of $I_c$ as a function of magnetic field show that the Josephson supercurrent can be detectable up to a field of 800 Oe. The observed monotonic decrease in $I_c$ with magnetic field and temperature is quantitatively explained with the framework of the quasiclassical theory of superconductivity. The developed technique opens up the possibility to fabricate nanowire-based complex hybrid structures consisting of normal and ferromagnetic parts to be used in superconducting spintronics.[40]

See supplementary material for a more detailed process of nanowires electrodeposition.

This work was supported in parts by Russian Foundation for Basic Research (RFBR) Grants Nos. 16-02-00815, 15-02-06743, 15-08-09012, and 16-38-00861 and by the Ministry of Education and Science of the Russian Federation (Grant No. 14Y.26.31.0007). M.K., V.R., and V.S. acknowledge partial support by the Program of Competitive Growth of Kazan Federal University and V.R., S.B., and M.K. appreciate partial support by the Increase Competitiveness Program of NUST "MISiS" (Research Project Nos. K2-2014-025 and K2-2016-051). In the part concerning the transport measurements at 20 mK, the work was supported by Russian Science Foundation (Grant No. 15-12-30030). We appreciate I. E. Batov for discussions and A. V. Knotko for TEM measurements.

[1]H. Courtois, P. Gandit, and B. Pannetier, Phys. Rev. B **52**, 1162 (1995).
[2]P. Dubos, H. Courtois, B. Pannetier, F. K. Wilhelm, A. D. Zaikin, and G. Schn, Phys. Rev. B **63**, 064502 (2001).
[3]J. J. A. Baselmans, B. J. van Wees, and T. M. Klapwijk, Phys. Rev. B **65**, 224513 (2002).
[4]J. Hanisch and G. Goll, J. Low Temp. Phys. **147**, 477 (2007).
[5]C. P. Garcia and F. Giazotto, Appl. Phys. Lett. **94**, 132508 (2009).
[6]M. Meschke, J. T. Peltonen, H. Courtois, and J. P. Pekola, J. Low Temp. Phys. **154**, 190 (2009).
[7]L. Angers, F. Chiodi, G. Montambaux, M. Ferrier, S. Guéron, H. Bouchiat, and J. C. Cuevas, Phys. Rev. B **77**, 165408 (2008).
[8]A. Ronzani, M. Baillergeau, C. Altimiras, and F. Giazotto, Appl. Phys. Lett. **103**, 052603 (2013).
[9]S. Samaddar, D. van Zanten, A. Fay, B. Sacépé, H. Courtois, and C. B. Winkelmann, Nanotechnology **24**, 375304 (2013).
[10]A. Ronzani, C. Altimiras, and F. Giazotto, Phys. Rev. Appl. **2**, 024005 (2014).
[11]R. N. Jabdaraghi, M. Meschke, and J. P. Pekola, Appl. Phys. Lett. **104**, 082601 (2014).
[12]A. Ronzani, C. Altimiras, and F. Giazotto, Appl. Phys. Lett. **104**, 032601 (2014).
[13]T. E. Golikova, M. J. Wolf, D. Beckmann, I. E. Batov, I. V. Bobkova, A. M. Bobkov, and V. V. Ryazanov, Phys. Rev. B **89**, 104507 (2014).
[14]T. E. Golikova, F. Hübler, D. Beckmann, N. V. Klenov, S. V. Bakurskiy, M. Yu. Kupriyanov, I. E. Batov, and V. V. Ryazanov, JETP Lett. **96**(10), 668 (2013).
[15]A. De Cecco, K. Le Calvez, B. Sacépé, C. B. Winkelmann, and H. Courtois, Phys. Rev. B **93**, 180505(R) (2016).
[16]R. N. Jabdaraghi, J. T. Peltonen, O.-P. Saira, and J. P. Pekola, Appl. Phys. Lett. **108**, 042604 (2016).
[17]H. Courtois, M. Mescheke, J. T. Peltonen, and J. P. Pekola, Phys. Rev. Lett. **101**, 067002 (2008).
[18]S. Shin and H. H. Cho, Electrochim. Acta **117**, 120 (2014).
[19]J. C. Cuevas, J. Hammer, J. Kopu, J. K. Viljas, and M. Eschrig, Phys. Rev. B **73**, 184505 (2006).
[20]J. C. Cuevas and F. S. Bergeret, Phys. Rev. Lett. **99**, 217002 (2007).
[21]F. S. Bergeret and J. C. Cuevas, J. Low Temp. Phys. **153**, 304 (2008).
[22]J. C. Hammer, J. C. Cuevas, F. S. Bergeret, and W. Belzig, Phys. Rev. B **76**, 064514 (2007).
[23]M. E. Toimil Molares, E. M. Höhberger, C. Schaeflein, R. H. Blick, R. Neumann, and C. Trautmann, Appl. Phys. Lett. **82**, 2139 (2003).
[24]P. YiTian and C. QuanFang, Mater. Sci. **58**, 3409 (2013).
[25]W. Gu, H. Choi, and K. Kim, Appl. Phys. Lett. **89**, 253102 (2006).
[26]C. Kim, W. Gu, M. Briceno, I. M. Robertson, H. Choi, and K. Kim, Adv. Mater. **20**, 1859 (2008).
[27]M. Jung, H. Noh, Y.-J. Doh, W. Song, Y. Chong, M.-S. Choi, Y. Yoo, K. Seo, N. Kim, B.-C. Woo, B. Kim, and J. Kim, ACS Nano **5**(3), 2271 (2011).
[28]A. Bid, A. Bora, and A. K. Raychaudhuri, Phys. Rev. B **74**(3), 035426 (2006).
[29]M. Mohl, P. Pusztai, A. Kukovecz, Z. Konya, J. Kukkola, K. Kordas, R. Vajtai, and P. M. Ajayan, Langmuir **26**, 16496 (2010).
[30]S. Zhong, T. Koch, M. Wang, T. Scherer, S. Walheim, H. Hahn, and T. Schimmel, Small **5**(20), 2265 (2009).
[31]W.-H. Xu, L. Wang, Z. Guo, X. Chen, J. Liu, and X.-J. Huang, ACS Nano **9**(1), 241 (2015).
[32]W. Park, D. V. Baxter, S. Steenwyk, I. Moraru, W. P. Pratt, Jr., and J. Bass, Phys. Rev. B **62**, 1178 (2000).

[33]K. D. Usadel, Phys. Rev. Lett. **25**, 507 (1970).
[34]K. S. Napolskii, P. J. Barczuk, S. Yu. Vassiliev, A. G. Veresov, G. A. Tsirlina, and P. J. Kulesza, Electrochim. Acta **52**, 7910 (2007).
[35]K. S. Napolskii, I. V. Roslyakov, A. A. Eliseev, D. I. Petukhov, A. V. Lukashin, S.-F. Chen, C.-P. Liu, and G. A. Tsirlina, Electrochim. Acta **56**, 2378 (2011).
[36]A. P. Leontiev, O. A. Brylev, and K. S. Napolskii, Electrochim. Acta **155**, 466 (2015).
[37]D. Brunel, D. Troadec, D. Hourlier, D. Deresmes, M. Zdrojek, and T. Mélin, Microelectron. Eng. **88**, 1569 (2011).
[38]R. Frielinghaus, I. E. Batov, M. Weides, H. Kohlstedt, R. Calarco, and T. Schäpers, Appl. Phys. Lett. **96**, 132504 (2010).
[39]H. Y. Günel, I. E. Batov, H. Hardtdegen, K. Sladek, A. Winden, K. Weis, G. Panaitov, D. Grützmacher, and T. Schäpers, J. Appl. Phys. **112**, 034316 (2012).
[40]V. S. Stolyarov, RU Patent 2 599 904 C1 (10 June 2016).